Pergamon

Int. J. Heat Mass Transfer. Vol. 38, No. 2, pp. 275–285, 1995
Copyright © 1994 Elsevier Science Ltd
Printed in Great Britain. All rights reserved
0017-9310/95 $9.50+0.00

0017-9310(94)00163-4

Three-dimensional linear stability of mixed-convective flow between rotating horizontal concentric cylinders

JUN YOUNG CHOI and MOON-UHN KIM†

Department of Mechanical Engineering, Korea Advanced Institute of Science and Technology, 373-1, Kusong-dong, Yusung-gu, Taejon 305-701, Korea

(*Received* 27 *January* 1994 *and in final form* 12 *May* 1994)

Abstract—The three-dimensional linear stability of the steady mixed-convective flow in a (moderately) wide gap annulus between two concentric horizontal cylinders with a heated rotating inner cylinder is studied numerically. The critical stability curves in the parameter plane of (Re^2, Gr) are determined. It is found that the effect of heating of inner cylinder postpones the formation of Taylor vortices when the rotation effect dominates the buoyancy effect. When the effect of buoyancy predominates over the effect of centrifugal force, the rotation of inner cylinder also stabilises the two-dimensional basic flow. When both rotation and buoyancy effects are important, the basic flow becomes unstable with respect to oscillatory disturbances. The results are in qualitative agreement with those of the three-dimensional numerical computations.

1. INTRODUCTION

Mixed convection in an annulus between heated rotating concentric cylinders has attracted considerable attention because of its wide technological applications such as cooling of rotating machinery or chemical vapour deposition processes. In the mixed convection system with a fixed radius ratio η, the flow and heat transfer characteristics are determined by the buoyancy and centrifugal force which are characterised by the Grashof number and (rotational) Reynolds number, respectively. Of particular relevance is the ratio Gr/Re^2, denoted by γ, which indicates the relative importance of the buoyancy and rotational effects.

From the late 1950s, a number of studies have been performed for heated rotating vertical annulus. While earlier works [1, 2] concentrated on the overall flow patterns and heat transfer rates, later studies focused on the stability [3–5] of the base flow which is steady, axisymmetric and independent of the axial coordinate, and on the subsequent development of the secondary flow and bifurcation phenomena [6, 7]. Recent stability analysis [5] shows that the destabilizing mode of base flow changes from axisymmetric mode through various spiral modes to axisymmetry mode as the Grashof number increases, and that the buoyancy has a stabilising effect except for large values of Prandtl number.

Several experimental investigations [8–10] of the mixed convection in a concentric horizontal annulus were reported, dealing with the overall heat transfer, but the problem received much less attention despite of its practical importance. Some investigators [11–13] conducted two-dimensional numerical experiments to study the flow patterns and heat transfer characteristics of the mixed convection in concentric or eccentric horizontal annulus with a heated rotating inner cylinder and stationary outer one. It has been observed [9] that the effect of natural convection decreases with the increase of the Reynolds number before the onset of the Taylor vortex motion. The results of two-dimensional computations also show that the overall heat transfer as well as the peak value of local heat transfer is reduced with increased rotation. On the other hand, once the Reynolds number is increased beyond the critical value and the Taylor vortex motion sets in, the overall heat transfer is observed to increase with the Reynolds number [8–10]. It is also found [10] that the free convection postpones the onset of Taylor vortex motion.

For the horizontal configuration, interaction of buoyancy and centrifugal effects is expected to produce fully three-dimensional flows when the centrifugal force is strong enough to trigger the formation of Taylor vortices. Recently, Yang and Farouk [14] performed a three-dimensional numerical analysis of flows and heat transfer in a horizontal concentric annulus. However, no investigation of the instability of two-dimensional mixed convective flows leading to three-dimensional flows has been carried out. Very recently, the present authors [15] examined the linear stability of the two-dimensional natural convection of air ($Pr = 0.71$) in a horizontal annulus of medium-sized gap ($0.5 < \eta < 0.8333$) against three-dimensional disturbances and obtained the critical Rayleigh

† Author to whom correspondence should be addressed.

NOMENCLATURE

$\mathbf{b}$	buoyancy force
C_B, C_M, C_R	critical stability curves
g	gravitational acceleration
Gr	Grashof number, $g\beta(T_i-T_o)L^3/\nu^2$
k	dimensionless axial wave number
$\mathbf{k}$	unit vector in axial direction
L	gap width of annulus, R_o-R_i
Pr	Prandtl number, ν/α
Q	representative variable for basic flow
q	representative variable for disturbance
$\mathscr{R}$	real part of complex number
Re	rotational Reynolds number, $\Omega_i R_i L/\nu$
R_i, R_o	radii of the inner and outer cylinders, respectively
r	dimensionless radial coordinate
s	complex growth rate, $s = s_r + is_i$
t	dimensionless time
V	characteristic velocity, $R_i\Omega_i$
$\mathbf{V}$	velocity for basic flow, $\mathbf{V} = (V_r, V_\phi, 0)$
$\mathbf{v}$	velocity, $\mathbf{v} = (v_r, v_\phi, v_z)$
z	dimensionless axial coordinate.

Greek symbols

α	thermal diffusivity
β	thermal expansion coefficient
γ	ratio of buoyancy to centrifugal force, Gr/Re^2
η	ratio of radii, R_i/R_o
Θ	temperature for basic flow
θ	temperature
λ	axial wavelength
ν	kinematic viscosity
ϕ	azimuthal coordinate
Ψ	stream function for basic flow
$\boldsymbol{\psi}$	vector potential, $\boldsymbol{\psi} = (\psi_r, \psi_\phi, \psi_z)$
Ω	vorticity for basic flow
$\boldsymbol{\omega}$	vorticity, $\boldsymbol{\omega} = (\omega_r, \omega_\phi, \omega_z)$
Ω_i	angular velocity of inner cylinder.

Subscripts

c	critical value
i, o	inner and outer cylinders, respectively
r, ϕ, z	radial, azimuthal and axial coordinates
s, p	two-dimensional steady basic flow and perturbation, respectively.

Superscript

*	complex conjugate.

numbers above which the basic flow is unstable. It was suggested that the instability is mainly caused by the buoyancy effects. It was found that the natural convective flow is stable for $\eta < 0.51$.

The present paper considers the linear stability of two-dimensional mixed-convective flow in a horizontal annulus of (moderately) wide gap width ($\eta = 0.6$ or 0.3846) against three-dimensional disturbances. The inner cylinder is rotating at a constant angular velocity while the outer cylinder is stationary. Both inner and outer cylinders are kept isothermal, the inner cylinder being hotter. The critical Grashof number as a function of the Reynolds number is obtained by integrating numerically the linearized disturbance equations under the suitably chosen initial conditions. The instability mechanism is discussed by examining the features of the critical disturbances. The two-dimensional basic mixed-convective flow is also obtained numerically. Computations are carried out in the range of $0 \leqslant Gr \leqslant 8500$ and $0 \leqslant Re \leqslant 170$ for a fluid of Prandtl number 0.71 (air).

For $\eta = 0.6$ (moderately wide gap annulus), the natural convection in the horizontal annulus is shown to be unstable for $Gr > 2810$ [15]. It is found that effects of rotation stabilise the buoyancy-dominated mixed convection ($\gamma > 0.33$) and that *the principle of exchange of stabilities* holds. For rotation-dominated flow ($\gamma < 0.16$), the critical mode is a stationary three-dimensional one and the critical Reynolds number increases with Grashof number. In the range $0.16 < \gamma < 0.33$, in which both rotation and buoyancy effects are important, the most unstable mode is found to be oscillatory, i.e. *the principle of exchange of stabilities* is upset by the competition between two destabilizing mechanisms, buoyancy and centrifugal instabilities.

For $\eta = 0.3846$ (wide gap annulus), similar instability phenomena are observed, although the instability mainly due to buoyancy effects does not occur in the range investigated ($Gr \leqslant 8500$). For rotation-dominated flow ($\gamma < 0.18$) the critical mode is stationary; in the range $0.18 < \gamma < 0.31$ the basic two-dimensional mixed convective flow becomes unstable to an oscillatory mode; and for $\gamma > 0.31$ the basic flow is stable.

2. MATHEMATICAL FORMULATION AND COMPUTATIONAL METHOD

Laminar mixed-convective flow in an infinite horizontal annulus between two concentric circular cylinders with inner and outer radii R_i and R_o is considered. Figure 1 shows the geometrical model and the cylindrical coordinate system (r, ϕ, z). The inner and outer cylinder surfaces are held at uniform temperatures T_i and T_o ($T_i > T_o$), respectively. The inner cylinder is rotating counterclockwise at a constant angular speed Ω_i. Adopting the Boussinesq approxi-

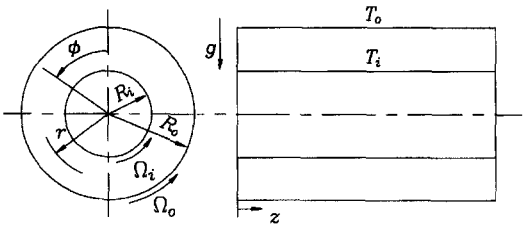

Fig. 1. Flow geometry and coordinates system.

mation and introducing the vector potential ψ such that:

$$\mathbf{v} = \nabla \times \psi, \tag{1}$$

the dimensionless governing equations in the vorticity–vector potential formulation [16] are written as:

$$\frac{\partial \omega}{\partial t} + (\mathbf{v}\cdot\nabla)\omega = (\omega\cdot\nabla)\mathbf{v} + \frac{1}{Re}\nabla^2\omega + \frac{Gr}{Re^2}\nabla\times\mathbf{b}, \tag{2}$$

$$\nabla^2\psi = -\omega, \tag{3}$$

$$\frac{\partial\theta}{\partial t} + (\mathbf{v}\cdot\nabla)\theta = \frac{1}{Re\,Pr}\nabla^2\theta, \tag{4}$$

where ω is the vorticity, $\mathbf{v}$ the velocity, $\mathbf{b} = (\theta\cos\phi, -\theta\sin\phi, 0)$ the buoyancy force, and θ the temperature. In this formulation, we obtain the solenoidal velocity field automatically, accordingly the discrete mass conservation at each time level is satisfied identically, and explicit appearance of the pressure is avoided. Equations (2)–(4) have been put into dimensionless form by taking $L\ (= R_o - R_i)$, $V\ (= R_i\Omega_i)$, L/V as characteristic length, velocity and time, respectively. Dimensionless temperature θ is defined by $\theta = (T - T_o)/(T_i - T_o)$. The non-dimensional parameters Gr, Re and Pr are defined by:

$$Gr = g\beta(T_i - T_o)L^3/\nu^2, \tag{5}$$

$$Re = VL/\nu, \tag{6}$$

$$Pr = \nu/\alpha, \tag{7}$$

where g is the gravitational acceleration, β the thermal expansion coefficient, α the thermal diffusivity and ν the kinematic viscosity.

The boundary conditions on rigid boundaries are expressed as [17]:

$$\left.\begin{array}{c} v_r = v_z = 0 \\ \partial(r\psi_r)/\partial r = \psi_\phi = \psi_z = 0 \\ \omega_r = 0 \quad \omega_\phi = -\partial v_z/\partial r \quad \omega_z = \partial v_\phi/\partial r \end{array}\right\} \text{ at } r = r_i, r_o, \tag{8}$$

$$v_\phi = 1 \quad \text{and} \quad \theta = 1 \quad \text{at} \quad r = r_i, \tag{9}$$

$$v_\phi = 0 \quad \text{and} \quad \theta = 0 \quad \text{at} \quad r = r_o, \tag{10}$$

where r_i and r_o are dimensionless radii of inner and outer cylinders.

2.1. *Two-dimensional basic flow equations*

For two-dimensional flow, the above equations (2)–(4) degenerate into the conventional vorticity–stream function formulation, by letting the z component of velocity equal to zero and all the variables be independent of z:

$$\mathbf{v} = \mathbf{V}(r,\phi,t) = (V_r, V_\phi, 0)$$

$$\omega = \Omega(r,\phi,t)\mathbf{k}$$

$$\psi = \Psi(r,\phi,t)\mathbf{k}$$

$$\theta = \Theta(r,\phi,t),$$

where $\mathbf{k}$ denotes the unit vector along z-axis.

The dimensionless governing equations for two-dimensional basic flow are given as

$$\frac{\partial\Omega}{\partial t} + V_r\frac{\partial\Omega}{\partial r} + V_\phi\frac{\partial\Omega}{r\partial\phi} = \frac{1}{Re}\nabla^2\Omega - \gamma\left(\frac{\partial\Theta}{\partial r}\sin\phi + \frac{\partial\Theta}{r\partial\phi}\cos\phi\right), \tag{11}$$

$$\nabla^2\Psi = -\Omega, \tag{12}$$

$$V_r = \frac{\partial\Psi}{r\partial\phi} \quad V_\phi = -\frac{\partial\Psi}{\partial r}, \tag{13}$$

$$\frac{\partial\Theta}{\partial t} + V_r\frac{\partial\Theta}{\partial r} + V_\phi\frac{\partial\Theta}{r\partial\phi} = \frac{1}{Re\,Pr}\nabla^2\Theta, \tag{14}$$

where $\gamma = Gr/Re^2$ denotes the ratio of buoyancy to centrifugal force.

Boundary conditions on the cylinder surfaces are written as follows:

$$\Psi = \Psi_i \quad \Omega = -\frac{\partial^2\Psi}{\partial r^2} + \frac{1}{r_i} \quad \Theta = 1 \quad \text{at} \quad r = r_i, \tag{15}$$

$$\Psi = 0 \quad \Omega = -\frac{\partial^2\Psi}{\partial r^2} \quad \Theta = 0 \quad \text{at} \quad r = r_o, \tag{16}$$

where Ψ_i is a constant to be determined by requiring that the pressure be single-valued in the annulus [18].

2.2. *Linear stability formulation*

In order to investigate the stability of the two-dimensional steady flow against three-dimensional small disturbances, we apply the standard methods of linear stability theory [19] following the procedures which Choi and Kim [15] used for the stability analysis of natural convection in a horizontal annulus.

All the variables of perturbed flow are written as the sum of the steady basic solution and the disturbances:

$$q(r,\phi,z,t) = Q_s(r,\phi) + \mathscr{R}[q_p(r,\phi,t)\exp(ikz)], \tag{17}$$

where k is the dimensionless axial wave number. Inserting expression (17) into equations (2)–(4), subtracting the basic steady parts and discarding $O(\varepsilon^2)$ and higher order terms, we obtain the following system of linear equations for the disturbances (dropping the subscripts s and p):

$$\frac{\partial \omega_r}{\partial t}+V_r\frac{\partial \omega_r}{\partial r}+V_\phi\frac{\partial \omega_r}{r\partial \phi}$$
$$=\omega_r\frac{\partial V_r}{\partial r}+\omega_\phi\frac{\partial V_r}{r\partial \phi}+\mathrm{i}k\Omega v_r$$
$$+\frac{1}{Re}\left(\nabla_*^2\omega_r-\frac{\omega_r}{r^2}-\frac{2}{r^2}\frac{\partial \omega_\phi}{\partial \phi}\right)+\mathrm{i}\gamma k\theta\sin\phi, \quad (18a)$$

$$\frac{\partial \omega_\phi}{\partial t}+V_r\frac{\partial \omega_\phi}{\partial r}+V_\phi\frac{\partial \omega_\phi}{r\partial \phi}+\frac{V_\phi\omega_r}{r}$$
$$=\omega_r\frac{\partial V_\phi}{\partial r}+\omega_\phi\frac{\partial V_\phi}{r\partial \phi}+\frac{\omega_\phi V_r}{r}+\mathrm{i}k\Omega v_\phi$$
$$+\frac{1}{Re}\left(\nabla_*^2\omega_\phi-\frac{\omega_\phi}{r^2}+\frac{2}{r^2}\frac{\partial \omega_r}{\partial \phi}\right)+\mathrm{i}\gamma k\theta\cos\phi, \quad (18b)$$

$$\frac{\partial \omega_z}{\partial t}+v_r\frac{\partial \Omega}{\partial r}+V_r\frac{\partial \omega_z}{\partial r}+v_\phi\frac{\partial \Omega}{r\partial \phi}+V_\phi\frac{\partial \omega_z}{r\partial \phi}=\mathrm{i}k\Omega v_z$$
$$+\frac{1}{Re}\nabla_*^2\omega_z-\gamma\left(\frac{\partial \theta}{\partial r}\sin\phi+\frac{\partial \theta}{r\partial \phi}\cos\phi\right), \quad (18c)$$

$$\nabla_*^2\psi_r-\frac{\psi_r}{r^2}-\frac{2}{r^2}\frac{\partial \psi_\phi}{\partial \phi}=-\omega_r, \quad (19a)$$

$$\nabla_*^2\psi_\phi-\frac{\psi_\phi}{r^2}+\frac{2}{r^2}\frac{\partial \psi_r}{\partial \phi}=-\omega_\phi, \quad (19b)$$

$$\nabla_*^2\psi_z=-\omega_z, \quad (19c)$$

$$v_r=\frac{\partial \psi_z}{r\partial \phi}-\mathrm{i}k\psi_\phi, \quad (20a)$$

$$v_\phi=-\frac{\partial \psi_z}{\partial r}+\mathrm{i}k\psi_r, \quad (20b)$$

$$v_z=\frac{\partial (r\psi_\phi)}{r\partial r}-\frac{\partial \psi_r}{r\partial \phi}, \quad (20c)$$

$$\frac{\partial \theta}{\partial t}+v_r\frac{\partial \Theta}{\partial r}+V_r\frac{\partial \theta}{\partial r}+v_\phi\frac{\partial \Theta}{r\partial \phi}+V_\phi\frac{\partial \theta}{r\partial \phi}=\frac{1}{Re\,Pr}\nabla_*^2\theta, \quad (21)$$

where

$$\nabla_*^2=\frac{\partial^2}{\partial r^2}+\frac{\partial}{r\partial r}+\frac{1}{r^2}\frac{\partial^2}{\partial \phi^2}-k^2.$$

The boundary conditions are homogeneous and given as:

$$\left.\begin{array}{c} v_r=v_\phi=v_z=\theta=0 \\ \partial(r\psi_r)/\partial r=\psi_\phi=\psi_z=0 \\ \omega_r=0\ \ \omega_\phi=-\partial v_z/\partial r\ \ \omega_z=\partial v_\phi/\partial r \end{array}\right\} \text{at } r=r_\mathrm{i}, r_\mathrm{o}. \quad (22)$$

Since the above linearized disturbance equations are homogeneous and do not depend on t explicitly, the solution will eventually show the exponential behaviour in time:

$$q_\mathrm{p}(r,\phi,t)\approx\tilde{q}(r,\phi)\,\mathrm{e}^{st}\quad s=s_\mathrm{r}+\mathrm{i}s_\mathrm{i}\quad t\gg 1, \quad (23)$$

where $\tilde{q}$ denotes the most unstable (least stable) mode of the eigenvalue problem resulting from the normal mode analysis of equations (18a)–(21). If $s_\mathrm{i}>0$ (or $s_\mathrm{i}<0$) at neutral stability ($s_\mathrm{r}=0$), the critical mode propagates in the negative (or positive) z-direction. It can be easily shown that if $(v_r, v_\phi, v_z, \psi_r, \psi_\phi, \psi_z, \omega_r, \omega_\phi, \omega_z, \theta)=(\tilde{v}_r, \tilde{v}_\phi, \tilde{v}_z, \tilde{\psi}_r, \tilde{\psi}_\phi, \tilde{\psi}_z, \tilde{\omega}_r, \tilde{\omega}_\phi, \tilde{\omega}_z, \tilde{\theta})\exp(st)$ is a solution of the linearized disturbance equations (18a)–(21) satisfying boundary conditions (22), then $(v_r, v_\phi, v_z, \psi_r, \psi_\phi, \psi_z, \omega_r, \omega_\phi, \omega_z, \theta)=(\tilde{v}_r^*, \tilde{v}_\phi^*, -\tilde{v}_z^*, -\tilde{\psi}_r^*, -\tilde{\psi}_\phi^*, \tilde{\psi}_z^*, -\tilde{\omega}_r^*, -\tilde{\omega}_\phi^*, \tilde{\omega}_z^*, \tilde{\theta}^*)\exp(s^*t)$ is also a solution. Here, quantities with tilde are complex-valued functions of r and ϕ, and the complex conjugate is denoted by the asterisk notation. This implies that when the critical disturbances are time-dependent ($s_\mathrm{i}\neq 0$) there is no preferred propagation direction. Also, standing waves may exist. In the numerical experiments, it has been found that the disturbances consist of both components moving in $+z$-direction and in $-z$-direction, when the critical mode is time-dependent.

2.3. *Computational procedures*

The basic flow and its stability are determined using the same numerical algorithm as in Choi and Kim [15]. For details, refer to ref. [15] and the references cited therein.

In the boundary conditions (15) for the basic flow, the constant Ψ_i cannot be given beforehand, and is determined from the condition of the single-valuedness of pressure on the wall [18]. The basic flow is assumed to reach a steady state when the difference between the results of consecutive time steps becomes less than 10^{-5} at every mesh point. In the whole range of parameters investigated ($Gr<8500$, $Re<170$), we were able to obtain the basic flow solutions which satisfy the steady-state criterion.

The linearized disturbance equations (18a)–(21) are integrated until the asymptotic exponential behaviour is established. Several complex-valued initial conditions which satisfy the no-slip and isothermal conditions on the cylinder walls are chosen. Final results are independent of the initial conditions. For a given axial wave number k and Grashof number Gr, the growth rate s_r and oscillating frequency s_i are determined from the time history of dependent variables which are, in general, complex-valued at several points in the domain. It is noticeable that both growth rate and oscillating frequency approach specific values after a sufficiently long time regardless of choice of the location (Fig. 2). As discussed in the previous subsection, the present algorithm can give only the magnitude of s_i. The transition Grashof number at which the growth rate s_r becomes zero is found by the method of false position. Usually four or five iterations are needed to obtain a transition Grashof number with the accuracy of at least three significant digits.

Approximate values of the critical Grashof number Gr_c and the critical wave number k_c for a given Reyn-

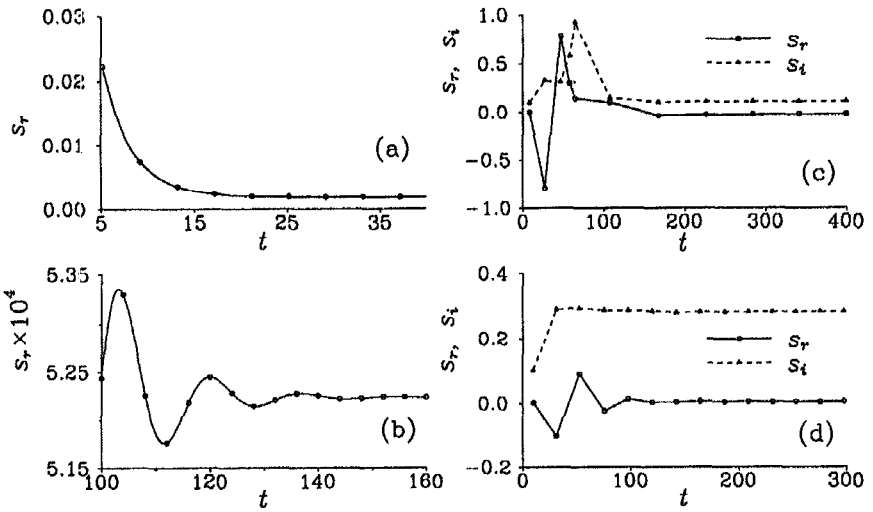

Fig. 2. Time history of s_r and s_i of θ for $\eta = 0.6$: (a) $Gr = 3620$, $Re = 20$, $k = 3.40$, $s_r = 1.84 \times 10^{-3}$, $s_i = 0.0$; (b) $Gr = 5845$, $Re = 100$, $k = 3.77$, $s_r = 5.22 \times 10^{-4}$, $s_i = 0.0$; (c) $Gr = 3239$, $Re = 100$, $k = 2.86$, $s_r = -2.15 \times 10^{-2}$, $s_i = 0.108$; (d) $Gr = 5380$, $Re = 140$, $k = 3.55$, $s_r = -4.00 \times 10^{-3}$, $s_i = 0.283$.

Table 1. Grid dependency test

Gap ratio	Grid (r, ϕ)	Re_c
$\sigma = 3$	20×64	2511.7
$(k = 3.05)$	20×128	2523.7
	30×64	2546.9
	30×128	2558.6
	40×64	2559.5
	40×128	2571.1
	50×128	2576.8
	50×256	2579.7
$\sigma = 1.25$	30×32	531.94
$(k = 3.37)$	30×64	491.14
	40×64	483.56
	40×128	483.89

olds number are determined from the minimum of the quadratic polynomial interpolation constructed from three pairs of wave number and transition Grashof number. The neutral stability curves in the plane of (Re^2, Gr) and the corresponding critical wave number curves have been explored in two ways, either by fixing the Reynolds number and changing Grashof numbers, or by fixing the Grashof number and changing Reynolds numbers, and the results were essentially the same. The curves are traced starting from the two points, the points of natural convection ($Re = 0$) and the isothermal Taylor–Couette flow ($Gr = 0$).

At each time level the unsteady calculation has been completely iterated to convergence, and sufficiently small time steps ($5 \times 10^{-3} \leqslant \Delta t \leqslant 2 \times 10^{-2}$) are used to produce time-accurate solutions. Calculations of both the basic flow and disturbance equations are based on the same grid system. Although the optimal grid system may depend on Gr, Re, σ and k, a uniform $(40 \times 128)(r, \phi)$ mesh is found to be adequate for $\eta = 0.6$ and (40×64) for $\eta = 0.3846$ from the grid dependency tests, the results of which are listed in Table 1. The computations were performed on a CRAY-2S supercomputer. Determination of a critical Grashof number (or Reynolds number) for a given radius ratio required a total CPU time of about 1 h.

Table 2. Comparison of critical Reynolds numbers of Taylor–Couette flow with inner rotating and outer stationary cylinders

η	k	Re_c (present method)	Re_c [20, 21]
0.75	3.135	85.30	85.78
0.6	3.150	71.39	71.72
0.5	3.165	68.00	68.19
0.4	3.184	68.00	68.30

3. COMPUTATIONAL RESULTS AND DISCUSSION

Computations were performed for two radius ratios ($\eta = 0.6$ and 0.3846) when the inner cylinder is kept hotter. The inner cylinder rotates counterclockwise at a constant angular velocity and the outer cylinder is at rest. It has been found [15] that in the absence of the rotation the two-dimensional natural convection is unstable with respect to a three-dimensional disturbance for $\eta = 0.6$ and stable for $\eta = 0.3846$. For $\eta = 0.3846$ (a wide gap annulus), some results of two-dimensional [12] and three-dimensional [14] computations have been reported.

To test the accuracy and reliability of the present algorithm, we applied the procedures to the stability problem of Taylor–Couette flow. Table 2 compares the critical Reynolds numbers computed by the present algorithm with those of Walowit *et al.* [20] and Takhar *et al.* [21]. The results are in good agree-

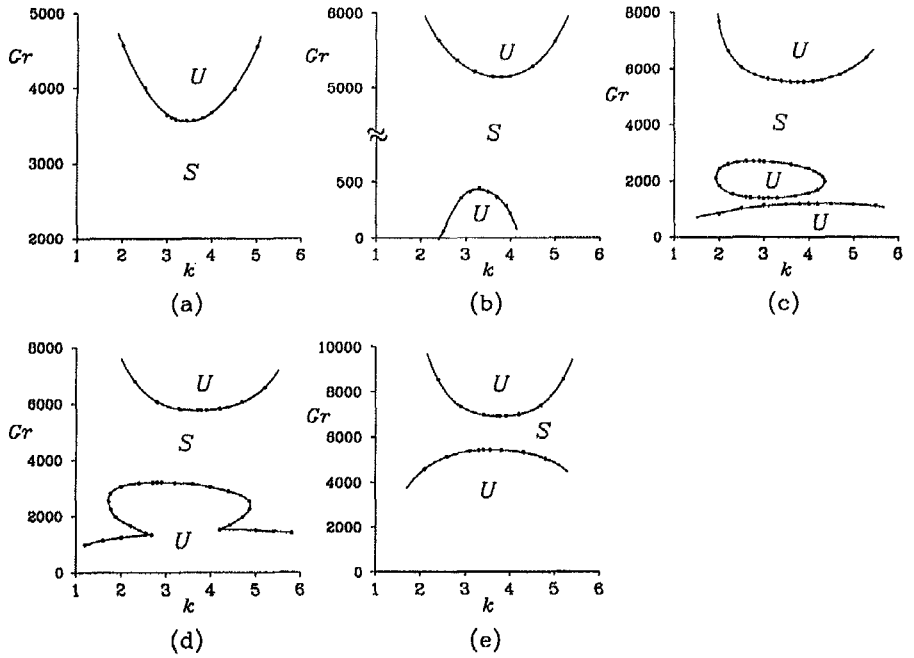

Fig. 3. Neutral stability curves for $\eta = 0.6$: (a) $Re = 20$; (b) $Re = 74$; (c) $Re = 90$; (d) $Re = 100$; (e) $Re = 140$. S and U indicate the stable and unstable regions, respectively.

ment. We have used the values of the axial wave numbers k presented in the references.

The computational procedures adopted in the present study can isolate only the most unstable (least stable) mode and require a large amount of time when two or more modes with nearly the same growth rate and different frequencies compete.

3.1. *Neutral stability curves*

We depict typical neutral stability curves for different values of Re for a moderately wide gap annulus ($\eta = 0.6$). Figure 3(a) shows the neutral stability curves of Gr vs k at $Re = 20$. The critical Grashof number Gr_c is 3558.4 and the critical wave number k_c is 3.443. The most unstable mode is stationary. Figure 4(a) displays the stream function and temperature distribution for the basic flow and distributions of the axial velocity and temperature disturbances. As seen in the figure, the disturbances are localized in a narrow region of upper-left part of the annulus where unstable density stratification of the basic flow is most pronounced. This implies that the instability is mainly caused by the buoyancy effects. This type of disturbances is designated by 'buoyancy-dominated' mode. As the Reynolds number decreases, the critical Grashof number decreases linearly towards 2810, the critical Grashof number for the natural convection [15]. The tendency that the increase of rotation postpones the instability due to buoyancy effects may be explained by considering that the peak value of local heat transfer rate (hence, the maximum adverse temperature gradient) decreases with increasing the rotational Reynolds number [12].

When the Reynolds number is increased above a critical value $Re_c \simeq 71.4$, which is the critical Reynolds number for the isothermal Taylor–Couette flow, a second branch appears. Figure 3(b) illustrates the neutral stability curves consisting of two branches at $Re = 74$. The basic flow is unstable for $Gr < Gr_1$ ($\simeq 439$) or $Gr > Gr_2$ ($\simeq 5143$). The multiple-valuedness of the critical Grashof number would imply the restabilization of the two-dimensional mixed convection with the increase of Gr. At a sufficiently low Grashof number ($Gr < Gr_1$), instability to a three-dimensional disturbance is encountered first. Increasing Gr above Gr_1, the two-dimensional basic flow would be restabilized and this flow will experience a second instability to a three-dimensional disturbance at a still higher Grashof number Gr_2. Neutral disturbances associated with the upper branch are of the same character as those associated with the neutral curve at $Re = 20$ [Fig. 3(a)], although the region of energetic disturbances is somewhat widened. On the other hand, stationary neutral disturbances associated with the lower branch, which are depicted in Fig. 4(b), are of entirely different character. Expanding the disturbance, say $\theta(r, \phi)$, into Fourier series:

$$\theta(r, \phi) = \theta_0(r) + \sum_{n=1}^{\infty} \{\theta_n^c(r) \cos n\phi + \theta_n^s(r) \sin n\phi\},$$

we find only the modes $n = 0$ and $n = 1$ are dominant and other modes are negligible. The neutral disturbances associated with the lower branch have a restricted number of significant non-axisymmetric modes (usually, $n \leqslant 2$). This type of disturbance will

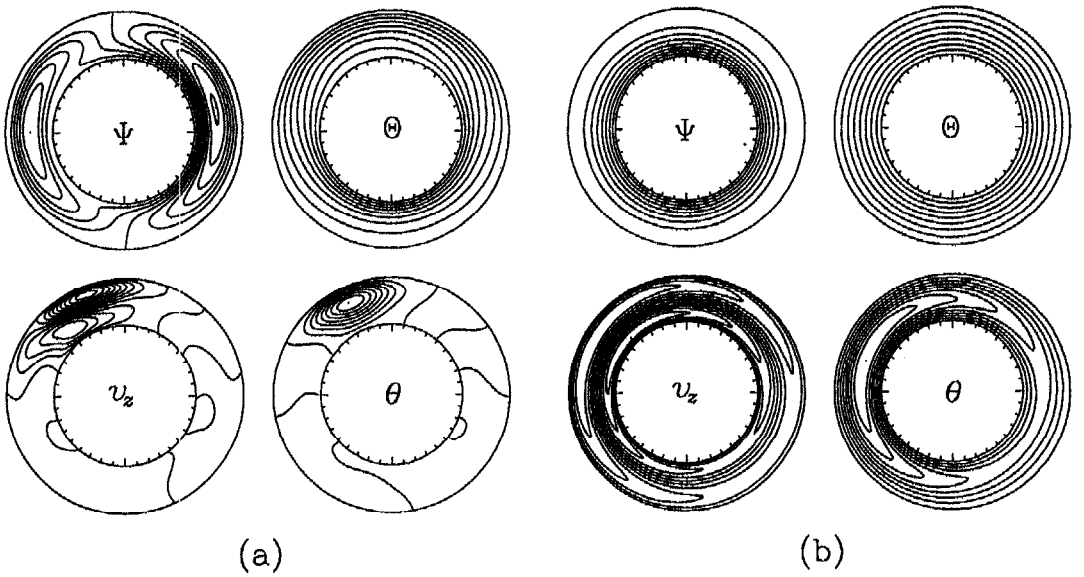

Fig. 4. Flow and temperature patterns for basic flows and disturbances for $\eta = 0.6$: (a) $Gr = 3620$, $Re = 20$, $k = 3.40$; (b) $Gr = 444$, $Re = 74$, $k = 3.22$.

be designated as 'rotation-dominated' mode. The critical Reynolds number for rotation-dominated mode decreases linearly towards 71.4 as Gr decreases. It is interesting to note that the most unstable mode of the basic two-dimensional mixed-convective flow is always three-dimensional, albeit that the effects of buoyancy on the basic flow are graphically invisible [Fig. 4(b)]. Numerical computation shows that the amplitude of the $n = 1$ spiral mode of rotation-dominated disturbance is as large as about one-tenth of that of axisymmetric mode ($n = 0$) even at $Gr = 10$.

Figure 3(c) plots the neutral stability curves at $Re = 90$. The flow is unstable for $Gr < Gr_1$ ($\simeq 1191$), Gr_2 ($\simeq 1390$) $< Gr < Gr_3$ ($\simeq 2701$) or $Gr > Gr_4$ ($\simeq 5517$). In the figure, in addition to upper and lower open-loop branches with which buoyancy-dominated and rotation-dominated modes are associated, respectively, a closed-loop branch appears. The neutral disturbances associated with the closed-loop branch are oscillatory. In Fig. 5, the time-dependent neutral temperature disturbance is shown at several instants during a period of oscillation. The region in which intense disturbances are observed is rather wide and swings forwards and backwards in the upper part of the annulus. We designate this type of disturbance as 'mixed-convective' mode. The closed-loop branch inside which the flow is unstable degenerates into a point at $Re = 77.8$ ($Gr = 1549, k = 2.947$) and minimum value of Gr of the closed-loop coincides with the maximum value of Gr of the lower open-loop at $Re = 93$ ($Gr = 1404$). As the Reynolds number is increased further, the closed-loop branch and the lower open-loop branch coalesce, leading to a lower open-loop branch [Fig. 3(d)]. The neutral modes associated with this branch consist of the oscillating mixed-convective mode for $1.72 < k < 4.85$ and the rotation-dominated mode for $k < 1.72$ or $k > 4.85$. Still increasing Re, the critical modes associated with the lower open-loop branch become solely oscillatory [Fig. 3(e)] in the range of k investigated ($1.2 < k < 6.0$). With the increase of Re, the maximum value of the Grashof number (Gr_1) of the lower branch approaches the minimum Grashof number (Gr_2) of the upper branch, and, at $Re \simeq 168$, Gr_1 and Gr_2 coincide ($Gr_1 = Gr_2 \simeq 8084.5$).

For the wide gap annulus ($\eta = 0.3846$), neutral stability curves show the same features as those for $\eta = 0.6$, except that the upper branches with which buoyancy-dominated modes are associated are absent. For $Re < 68.4$, the basic two-dimensional mixed-convective flow is stable; for $68.4 < Re < 82.1$, an open-loop branch below which the flow is unstable appears; for $82.1 < Re < 98$, a closed-loop branch inside which the flow is unstable appears; and, for $Re > 98$, the closed-loop branch and the lower open-loop branch coalesce. Figure 6 depicts the neutral stability curves at $Re = 90$.

3.2. *Critical stability results*

Figure 7 displays the critical stability diagrams for $\eta = 0.6$. In Fig. 7(a), the critical values of the Grashof number are plotted as a function of Re^2. The stable regime is bounded by three marginal curves, designated by C_B, C_M and C_R, along which the critical modes are identifiable as buoyancy-dominated, mixed-convective and rotation-dominated modes, respectively. Along C_R (rotation-dominated stability boundary) the critical Reynolds number for $Gr > 0$ (mixed convection) is larger than that for $Gr = 0$ (isothermal Taylor–Couette flow) and increases monotonically with Gr. It can be, thus, concluded that the free convection in the horizontal annulus delays the

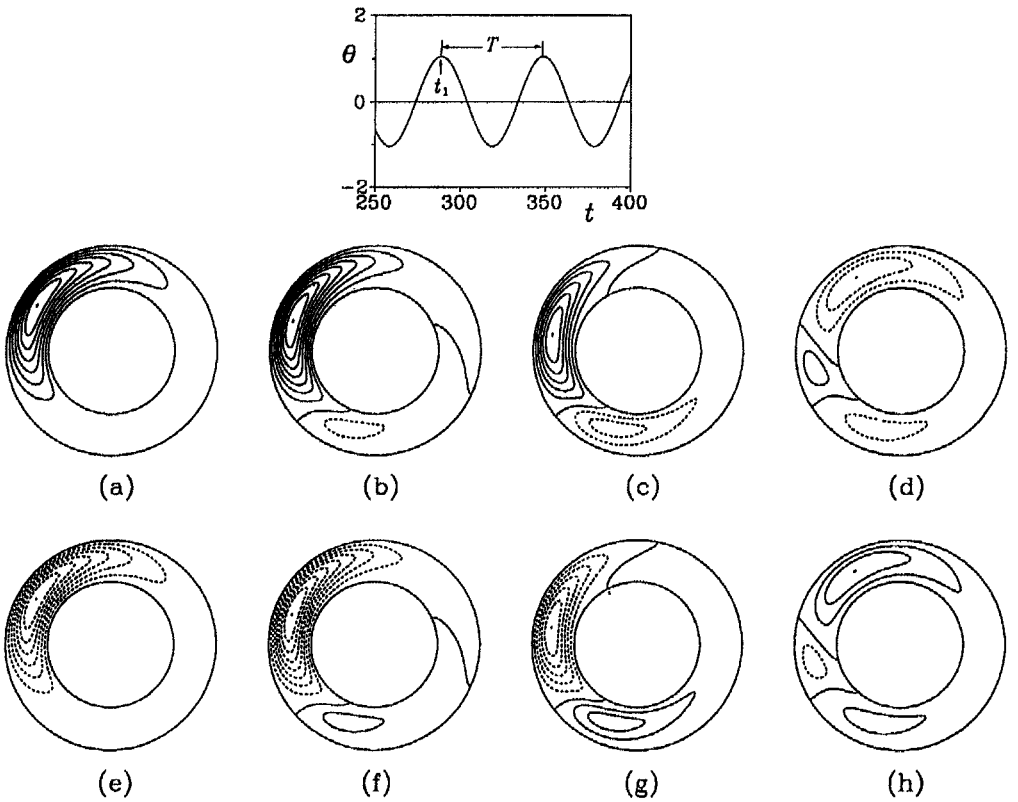

Fig. 5. Distributions of disturbance temperature at several instants during a period of oscillation for $\eta = 0.6$, $Re = 90$ and $Gr = 2700$: (a) $t = t_1$, $(\theta_{min}, \theta_{max}) = (0.00, 3.33)$; (b) $t_1 + T/8$, $(-0.43, 4.01)$; (c) $t_1 + 2T/8$, $(-0.77, 2.63)$; (d) $t_1 + 3T/8$, $(-1.32, 0.30)$; (e) $t_1 + 4T/8$, $(-3.33, 0.00)$; (f) $t_1 + 5T/8$, $(-4.01, 0.43)$; (g) $t_1 + 6T/8$, $(-2.62, 0.77)$; (h) $t_1 + 7T/8$, $(-0.29, 1.33)$. $T = 2\pi/s_i \simeq 59.84$. Dotted lines represent negative disturbance isotherms.

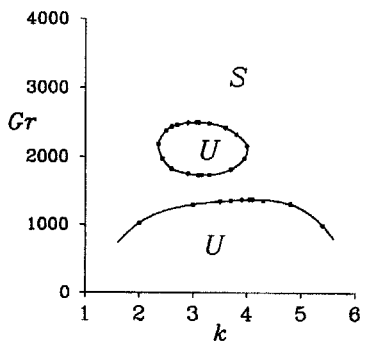

Fig. 6. Neutral stability curves for $\eta = 0.3846$ and $Re = 90$. S and U indicate the stable and unstable regions, respectively.

formation of Taylor vortices, which is in accordance with the experimental observation [10]. Rotation effects also stabilize the convective flow, since the critical Grashof number on buoyancy-dominated stability boundary (C_B) increases with the Reynolds number. On the curves C_B and C_R the critical disturbances are stationary ($s_i = 0$), whereas on C_M the critical states are time-dependent ($s_i \neq 0$). At the point $A \approx (93^2, 1404)$, the stationary rotation-dominated branch C_R and the oscillatory mixed-convective branch C_M intersect and the point $B \approx (168^2, 8084.5)$ represents the intersection of the stationary buoyancy-dominated branch C_B with C_M. At these points stationary and oscillatory states may coexist. Bifurcation phenomena for which the most unstable mode switches from a stationary mode to a time-dependent mode are not uncommon, when two or more effects characterize the stability of the flow: to cite a few, Taylor–Dean problem [22], rotating curved channel flow [23] and electrohydrodynamic thermal instability flow [24], etc.

Figure 7(b) shows the critical axial wave number k_c as a function of Re^2. For rotation-dominated modes, instability wave number k_c (wavelength λ_c) increases (decreases) gradually from $k_c \simeq 3.145$ ($\lambda_c \simeq 2.0$) for isothermal Taylor vortex flow to $k_c \simeq 4.3$($\lambda_c \simeq 1.5$) as the buoyancy effect increases. On the other hand, for heated rotating vertical annulus, the opposite trend has been observed [5]: wavelengths of successive helical modes grow continuously and then suddenly shrink when another spiral mode of higher azimuthal wave number evolves. For buoyancy-dominated modes, critical axial wave numbers rapidly approach a nearly constant value of $k_c \simeq 3.77$ as Re^2 increases. At points A and B, the critical wave number changes discontinuously.

In Fig. 7(c), the frequency s_i of the critical neutral

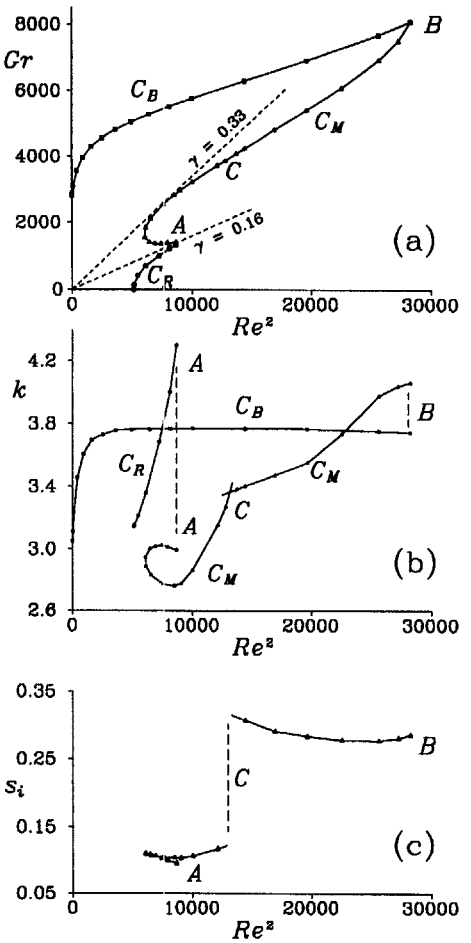

Fig. 7. Critical stability diagrams as functions of Re^2 for $\eta = 0.6$: (a) critical stability curves; (b) critical wave numbers; (c) oscillation frequencies. C_R denotes the rotation-dominated branch, C_B the buoyancy-dominated branch and C_M the mixed-convective branch. Points A and B represent the bifurcation points at which stationary and oscillatory states may coexist and C the point at which two different oscillatory states coexist.

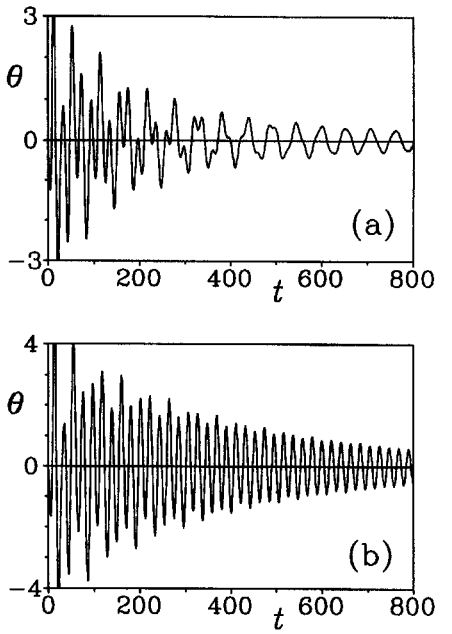

Fig. 8. Time history of disturbance temperatures at points near the bifurcation point C: (a) $Gr = 3732$, $Re = 110$, $k = 3.15$; (b) $Gr = 4268$, $Re = 120$, $k = 3.40$. Estimated oscillation frequencies are $s_i = 0.117$ for (a) and $s_i = 0.295$ for (b).

disturbance associated with the curve C_M is plotted as a function of Re^2. It is observed that there exists a bifurcation point $C \approx (115^2, 3960)$ at which two time-dependent modes of different frequencies coexist. At the bifurcation point C, the wave number of the critical mode seems to change discontinuously. Since discontinuity is very weak, however, the evaluation of the precise value of the jump by the present method is extremely difficult and not attempted. Figure 8 shows temporal variations of disturbance temperatures at points near the bifurcation point C. As shown in the figure, the beat of two modes continues for a long time before the predominant mode settles down ultimately.

Figure 9 displays the stability boundaries in (Re^2, Gr) plane and the corresponding critical axial wave number and oscillating frequency as functions of Re^2 for the radius ratio of $\eta = 0.3846$. The overall features of these curves closely resemble those of Fig. 7, except that the critical curve for buoyancy-dominated modes is absent. The absence of the buoyancy-dominated critical modes is not unexpected since the two-dimensional natural convective flow is predicted to be stable with respect to three-dimensional disturbances when the gap is wide [15]. At point $A \approx (98^2, 1790)$, the stationary rotation-dominated critical mode and the oscillatory mixed-convective mode coexist, and point $C \approx (113^2, 3559)$ represents the bifurcation point at which two different time-dependent modes coexist. An appreciable jump in wave number as well as the frequency of the critical disturbances is observed at C. Yang and Farouk [14] have conducted the three-dimensional numerical computations for the mixed convection in an annulus of finite axial length (axial length/gap width = 6) for $\eta = 0.3846$. They presented the results that at a fixed Reynolds number ($Re^2 = 10000$), which is sufficient to trigger the Taylor vortex in an isothermal annulus, the flow is essentially two-dimensional for $Gr = 6944$, whereas the Nusselt number distributions for $Gr = 138$ and 1388 show a wave-like variation in the axial direction, suggesting the presence of Taylor cells. They concluded that the critical Reynolds number for the onset of the Taylor cells would be higher than 100 at $Gr = 6944$. Calculation for a fixed Grashof number ($Gr = 2777$) with varying Reynolds number suggested that the onset of rotational instability occurs somewhere between $Re = 80$ and 130, but determination of the precise value of the critical Reynolds number was not attempted. The present analysis gives $Re_c = 153$ at $Gr = 6944$ and $Re_c = 96$ at $Gr = 2777$, indicating that the results of the present linear stability

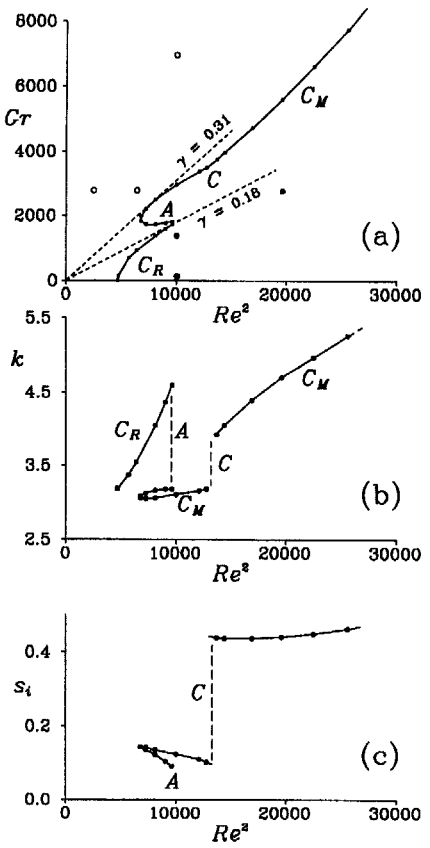

Fig. 9. Critical stability diagrams as functions of Re^2 for $\eta = 0.3846$: (a) critical stability curves—at points indicated by open circles computational results by Yang and Farouk [14] give the two-dimensional flow and at points indicated by filled circles the flow is three-dimensional; (b) critical wave numbers; (c) oscillation frequencies.

analysis and the three-dimensional numerical analysis, taking into account full non-linear effects, are not inconsistent.

From Figs. 7(a) and 9(a), it is inferred that the characteristics of the linear instability of the two-dimensional mixed convection in a (moderately) wide horizontal annulus can be approximately delineated by the ratio $\gamma = Gr/Re^2$ for fixed values of the radius ratio η. In a moderately wide annulus ($\eta = 0.6$), the mode type of the most unstable disturbances changes from the stationary rotation-dominated mode ($\gamma < 0.16$) through the oscillatory mixed-convective mode ($0.16 < \gamma < 0.33$) to the stationary buoyancy-dominated mode ($\gamma > 0.33$) as γ increases. In a wide annulus ($\eta = 0.3846$), the onset of hydrodynamic instabilities is caused by the stationary rotation-dominated mode for $\gamma < 0.18$ and by the oscillatory mixed-convective mode for $0.18 < \gamma < 0.31$. At higher values of γ, two-dimensional basic flow is stable in the range of parameters investigated ($Re < 170, Gr < 8500$). The results of two-dimensional computations reported by Fusegi *et al.* [12] may be legitimated, thus, in that the present analysis suggests that the two-dimensional mixed convections in the parameter range ($\gamma > 1$) they investigated may certainly be stable to three-dimensional disturbances. On the other hand, a part of the results reported by Lee [11, 13] might be experimentally not observable, since his study includes parameter combinations for which two-dimensional flows are unstable to three-dimensional disturbances.

4. CONCLUSIONS

The three-dimensional linear stability of mixed-convective flow in a horizontal concentric annulus with a heated rotating inner cylinder is studied numerically for a fluid of Prandtl number 0.71 (air). Computations are carried out for a moderately wide annulus ($\eta = 0.6$) and for a wide annulus ($\eta = 0.3846$).

The main results are displayed in Figs. 7 and 9. The natural convection is found to postpone the formation of Taylor vortices, when the effect of rotation dominates the effect of buoyancy. This tendency is in agreement with experimental observation [10]. When the effect of buoyant forces predominates over the effect of centrifugal forces, the rotation of the inner cylinder stabilizes the natural convective flow in the horizontal annulus. Since the two-dimensional steady natural convection in a wide annulus ($\eta < 0.51$) is stable to small three-dimensional disturbances [15], it is not unexpected that the basic flow in the annulus of $\eta = 0.3846$ is stable when the Grashof number is large enough compared with the Reynolds number ($Gr/Re^2 > 0.31$). When both the buoyancy effect and the rotation effect are important, the basic flow becomes unstable with respect to oscillatory disturbances.

Stability boundaries are composed of stationary and oscillatory branches. At intersection points of the branches, the present linear analysis predicts two distinct critical modes. However, to clarify which modes can be observed in the vicinity of the intersection points, the analysis of non-linear interactions is needed [24, 25].

No experimental study on the stability of the mixed convection in a horizontal annulus has been reported so far, in contrast with the stability of the circular Couette flow in a heated vertical annulus. It is hoped that the present work will stimulate experimental investigations.

Acknowledgements—The authors would like to thank the computational resources provided by Samsung Electronics Co. Ltd. and the support from AFERC (Advanced Fluid Engineering Research Center).

REFERENCES

1. I. S. Bjorklund and W. M. Kays, Heat transfer between concentric rotating cylinders, *J. Heat Transfer* **81**, 175–186 (1959).
2. K. M. Becker and J. Kaye, Measurements of diabatic flow in an annulus with an inner rotating cylinder, *J. Heat Transfer* **84**, 97–105 (1962).

3. K. M. Becker and J. Kaye, The influence of a radial temperature gradient on the instability of fluid flow in an annulus with an inner rotating cylinder, *J. Heat Transfer* **84,** 106–110 (1962).
4. H. A. Snyder and S. K. F. Karlsson, Experiments on the stability of Couette motion with a radial thermal gradient, *Phys. Fluids* **7,** 1696–1706 (1964).
5. M. Ali and P. D. Weidman, On the stability of circular Couette flow with radial heating, *J. Fluid Mech.* **220,** 53–84 (1990).
6. K. S. Ball and B. Farouk, On the development of Taylor vortices in a vertical annulus with a heated rotating inner cylinder, *Int. J. Numer. Meth. Fluids* **7,** 857–867 (1987).
7. K. S. Ball and B. Farouk, Bifurcation phenomena in Taylor–Couette flow with buoyancy effects, *J. Fluid Mech.* **197,** 479–501 (1988).
8. F. Tachibana, S. Fukui and H. Mitsumura, Heat transfer in an annulus with an inner rotating cylinders, *Bull. J.S.M.E.* **3,** 119–123 (1960).
9. A. Aoki, H. Nohira and H. Arai, Convective heat transfer in an annulus with an inner rotating cylinder, *Bull. J.S.M.E.* **10,** 523–532 (1967).
10. S. R. M. Gardiner and R. H. Saberskey, Heat transfer in annular gap, *Int. J. Heat Mass Transfer* **21,** 1459–1466 (1978).
11. T. S. Lee, Numerical experiments with laminar fluid convection between concentric and eccentric heated rotating cylinders, *Numer. Heat Transfer* **7,** 77–87 (1984).
12. T. Fusegi, B. Farouk and K. S. Ball, Mixed-convection flows within a horizontal concentric annulus with a heated rotating inner cylinders, *Numer. Heat Transfer* **9,** 591–604 (1986).
13. T. S. Lee, Numerical computation of fluid convection with air enclosed between the annuli of eccentric heated horizontal rotating cylinders, *Computers Fluids* **21,** 355–368 (1992).
14. L. Yang and B. Farouk, Three-dimensional mixed convection flows in a horizontal annulus with a heated rotating inner circular cylinder, *Int. J. Heat Mass Transfer* **35,** 1947–1956 (1992).
15. J. Y. Choi and M.-U. Kim, Three-dimensional linear stability of natural convective flow between concentric horizontal cylinders, *Int. J. Heat Mass Transfer* **36,** 4173–4180 (1993).
16. K. Aziz and J. D. Hellums, Numerical solution of the three-dimensional equations of motion for laminar natural convection, *Phys. Fluids* **10,** 314–324 (1967).
17. G. J. Hirasaki and J. D. Hellums, A general formulation of the boundary conditions on the vector potential in three-dimensional hydrodynamics, *Quart. J. Appl. Math.* **26,** 331–342 (1968).
18. J. H. Adlam, Computation of two-dimensional time-dependent natural convection in a cavity where there are internal bodies, *Computers Fluids* **14,** 141–157 (1986).
19. P. G. Drazin and W. H. Reid, *Hydrodynamic Stability*. Cambridge University Press, New York (1981).
20. J. Walowit, S. Tsao and R. C. Di Prima, Stability of flow between arbitrarily spaced concentric cylindrical surfaces including the effect of a radial temperature gradient, *J. Appl. Mech.* **31,** 585–593 (1964).
21. H. S. Takhar, M. A. Ali and V. M. Soundalgekar, Stability of the flow between rotating cylinders—wide-gap width, *J. Fluids Engng* **111,** 97–99 (1989).
22. I. Mutabazi, J. J. Hegseth and C. D. Andereck, Pattern formation in the flow between two horizontal coaxial cylinders with a partially filled gap, *Phys. Rev. A* **38,** 4752–4760 (1988).
23. O. J. E. Matsson and P. H. Alfredsson, Curvature- and rotation-induced instabilities in channel flow, *J. Fluid Mech.* **210,** 537–563 (1990).
24. H.-J. Ko and M.-U. Kim, Electrohydrodynamic convective instability in a horizontal fluid layer with temperature gradient, *J. Phys. Soc. Japan* **57,** 1650–1661 (1988).
25. K. Fujimura and R. E. Kelly, Mixed mode convection in an inclined slot, *J. Fluid Mech.* **246,** 545–568 (1993).